Near-infrared Image Enhancement Method in IRFPA Based on Steerable Pyramid

Qinghe Zheng, Xinyu Tian, Mingqiang Yang and Shi Liu

***Abstract*—Near-infrared imaging mainly uses near-infrared band ambient light imaging reflected by the target, which has better atmospheric penetration performance and human skin penetration performance than visible light imaging. Therefore, near-infrared imaging is widely used in military, medical and many industrial production. Aiming at reducing the noise and improving the contrast of the near-infrared images gained from infrared focal plane array (IRFPA), the near-infrared image enhancement method based on steerable pyramid is proposed in this paper. First of all, the near-infrared image is decomposed into multi-scales using the steerable pyramid model; then the coefficients of low-frequency and high-frequency of the image are obtained. In order to improve the contrast of the original near-infrared image, the coefficients with low-frequency are nonlinearly transformed through fuzzy-set theory. Then the coefficients of high-frequency are dealt with threshold method to reduce the noise. Next, these images are reconstructed. At last, anti-sharpening mask is used to highlight the details of the image. During the reconstruction, a adaptive interpolation algorithm is put forward to resolve the distortion problem in the steerable pyramid algorithm. The experimental results show that this algorithm has a good effect on the enhancement of near-infrared images, and significantly improves the quality of near-infrared image produced by IRFPA device. The comparison results with various algorithms show that our algorithm outperforms the state-of-art in terms of contrast gain, comentropy, mean-square error, and peak signal to noise ratio. The experimental results illustrate that the proposed algorithm can efficiently enhance the near-infrared image.**

***Index Terms*—near-infrared image enhancement, steerable pyramid decomposition, fuzzy set, adaptive interpolation**

Fig. 1. The near-infrared image enhancement results for three scenes. The first column represents the original near-infrared image and the second column represents the enhanced image.

I. Introduction

With the rapid development of science and technology, new imaging methods continue to emerge. In recent years, the transmission characteristics of near-infrared light with a wavelength of 600-1300 nm in biological tissues and near-infrared light imaging have become the hot spots in biomedical photonics research [24], [25], [26], [27], [28], [29]. Near-infrared image refers to the sample formed by reflecting or irradiating the near-infrared spectrum segment with the target received by the remote sensor. It belongs to a new type of imaging technology and is still in the stage of exploration and development. Near-infrared imaging mainly uses near-infrared band ambient light reflected by the target, which has better atmospheric penetration performance and human skin penetration performance than that of the visible light imaging method. Therefore, the near-infrared imaging is used in military, medical and many industrial production. As a result, the research and development of near-infrared imaging is of great significance, and it has potential significance in the early diagnosis of medical problems such as cancer diagnoses and cardiovascular and cerebrovascular diseases. Therefore, studying and exploring near-infrared imaging technology and enhancing near-infrared images are of great significance for near-infrared detection.

The near-infrared imager (system NIR-50) is currently the mainstream imaging device in IRFPA, but due to hardware

Manuscript received October 13, 2018; revised January 11, 2019. This work was supported by the Fundamental Research Funds of Shandong University (Grant 2018JC040), National Natural Science Foundation of China (Grant 61571275), and Sub-project of the National Key Research and Development Program of China (Grant 2018YFF01014304).

Qinghe Zheng and Shi Liu are with the School of Information Science and Engineering, Shandong University, Qingdao 266237, China (e-mail: 15005414319@163.com, 1551837188@qq.com)

Mingqiang Yang (corresponding author) is with School of Information Science and Engineering, Shandong University, Jimo, Qingdao 266237, China (e-mail: yangmq@sdu.edu.cn.com).

Xinyu Tian is with College of Mechanical and Electrical Engineering, Shandong Management University, Changqing, Jinan 250357, Shandong, China (e-mail: 18769796159@163.com).

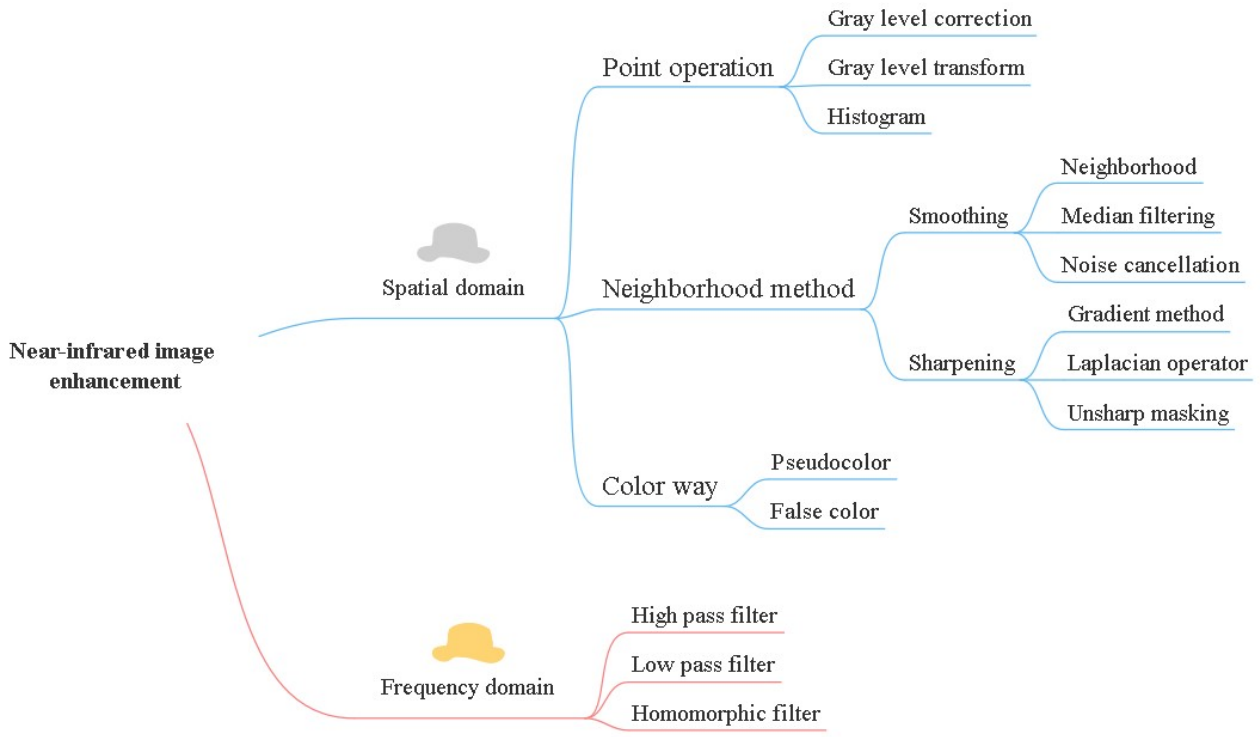

Fig. 2. Related work in the spatial domain and frequency domain of near-infrared image enhancement.

limitations and the environmental changes, the near-infrared image of IRFPA has the following disadvantages compared to the light image:

- Low resolution.
- Complex noise.
- Low contrast.
- Low signal to noise ratio.
- Blurred visual effects.
- Non-linear relationship between gray distribution and target reflection characteristics.

Therefore, image enhancement algorithm used for image processing and improving image quality is an essential step in the practical application of equipment. Image enhancement algorithms are divided into spatial domain enhancement [16] and frequency domain enhancement [17]. Spatial domain enhancement directly deals with pixel gray value. The main methods include grayscale stretch [1], histogram equalization [2], and anti-sharpening mask [3]. Histogram equalization can improve image contrast to a certain extent, but at the same time, image noise is also enhanced, and the overall effect is not ideal. The anti-sharpening mask enhances the edge of the image, but the noises are also enhanced too. The frequency domain based enhancement method first transforms the image into the frequency domain, and then the frequency domain filters are used to enhance the image. It mainly includes low pass filtering method [15], high pass filtering method [18] and homomorphic filtering method [19]. Single frequency domain enhancement method is difficult to reconcile image noise and edge processing: good denoising often results in the loss of image details.

In recent years, in view of the actual engineering [7] and computational requirements [8], Li [4] has proposed adaptive detail enhancement of infrared images based on the sub-band decomposition multiscale (*i.e.*, Retinex) [9], which can better enhance the details of the highlighting and dark areas of the image. Yun *et al.* [5] proposed that the near-infrared image enhancement method combined with histogram equalization and fuzzy set theory can mainly enhance image contrast. But the above two methods cannot deal with the ubiquitous noise problem in near-infrared images. Jia *et al.* [6] proposed that the near-infrared image enhancement algorithm based on the generalized linear operation and bilateral filtering is mainly aimed at eliminating the bad halo in near-infrared images.

Although these methods have achieved some results, they cannot solve the problem of complex noises and low contrast in NIR-50 near infrared imager. Therefore, a near-infrared image enhancement method based on steerable pyramid is proposed in this paper. Steerable pyramid is one of the most famous direction controlled pyramid model, which can deal with image information at multiple scales. The model has translation invariance, rotation invariance and multi direction. It can better describe the feature of curved edge in the image and retain the details of the image. In the process of sampling, an adaptive interpolation algorithm is proposed to solve the distortion problem of steerable pyramid based method in the interpolation process. The experimental results show that this algorithm has the good enhancement effect on near-infrared images. The comparison results with various methods show that our algorithm outperforms the state-of-the-art in terms of the contrast gain, comentropy, mean-square error, and peak signal to noise ratio. The image enhancement results for some example scenes are shown in Fig. 1.

The rest of the paper is organized as the follows. We first introduce and analyze some related works of near-infrared image enhancement in Section II. The details and operation flow of near-infrared image enhancement method in IRFPA are then presented in Section III. Experimental results and corresponding analysis are introduced in Section IV. Finally, we discuss what we learned, our conclusions, and the future works in Section V.

II. Related Works

Image enhancement is one of the pivotal issues in image processing research [20], [21], [30], [31]. The effect can be judged according to human perception and understanding of the resulting image on the display (or image). Therefore, the image enhancement algorithm should consider the visual characteristics of the human eye. Physiological vision studies [22], [23], [32], [33] have found that the cellular connections between the retinal pyramidal cells and the brain's visual skin can be divided into two opposing systems, *i.e.*, ON and OFF. Both respond to light intensity in the opposite direction: the ON system is sensitive to the increase in light intensity, while the OFF system is sensitive to the reduction in light intensity. These two different responses make the vision system most sensitive to external contrast changes, and therefore can be used to deal with and optimize the processing procedure of visual information in the cerebral cortex. Specifically, the "structured" image of the human eye with more detail is more sensitive than the voucher image without detail, and the visibility of noise in the "structured" image is also lower than in the flat image. When the image is enhanced in detail by a magnitude greater than the amplitude of the flat image, an overall image enhanced visual effect will be obtained.

Near infrared imaging began in the late 1980s. At present, near infrared imaging has been applied to the cardiovascular surgery, breast detection, brain functional imaging and so on. Near infrared imaging relies on the selective absorption of near-infrared light in biological groups. At present, there are two ways of near-infrared imaging: transmission imaging and tomography. After the light passes through tissue, projection images and tomographic images are formed on the imaging plane. According to the different light sources, near-infrared imaging can be divided into three modes: continuous wave method, frequency domain method and time domain method [34]. The continuous wave technology uses a light intensity constant light source to directly irradiate the tissue to be detected, and then capture the light intensity within a certain range of the tissue surface through the image acquisition equipment to form the near infrared image. Frequency domain method uses high frequency near infrared light as light source. Generally, the time domain based method uses picosecond or femtosecond ultrashort laser pulses to irradiate tissue. Then, the relationship between the intensity and time of the light is measured with a picosecond resolution camera at a distance from the incident point.

At present, there are many image enhancement algorithms, which can be broadly divided into two major classes: global enhancement and local enhancement. Global enhancement is designed to achieve contrast enhancement by changing the overall brightness in accordance with certain rules, such as increasing brightness and brightness when the image is too dark. Typical algorithms have histogram equalization, linear or nonlinear stretching of brightness [34], [35], [36]. The global enhancement algorithm is relatively simple, but the global enhancement is only suitable for the images with low overall contrast. Actually, the local enhancement algorithm can improve global enhancement [37], [38]. It can be flexibly operated locally with a better overall performance than the global enhancement methods. In contrast, local enhancement can theoretically achieve enhancement in any situation, but the search for local enhancement operator is difficult, and the implementation in multiple complex situations is much more

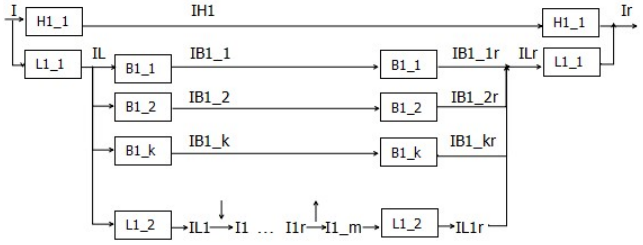

Fig. 3. Block diagram of steerable pyramid.

complicated than global enhancement. In recent years, people have also proposed algorithms that are different from local and global enhancements, placing emphasis on the edge (or high-frequency details) rather than on the change in the grayscale brightness of the area. Due to the human eye's sensitivity to high-frequency information, it is also true from the point of view of the physiological vision through high frequency information transmission. And this edge based enhancement is more targeted and more advantageous than the previous algorithm, such as multi-scale edge enhancement algorithms recently emerged: SSR (single-scale Retinex) [4], MSR (multi-scale Retinex) [5], wavelet enhancement [6] and the surface waves proposed by Starch [7] (Curvelet) enhanced algorithms and so on. Yang (image enhancement based on fractional differential image) adopts the image enhancement method based on fractional differential operator. The visual effect of the enhanced image is obviously better than that of the traditional differential sharpening (integer differential) method. Starch et al has proved that surface wave (Curvelet) enhancement algorithm is better than SSR, MSR algorithm and wavelet enhancement algorithm.

In 1998, the American scholar E. Huang [8] proposed an empirical mode decomposition algorithm used to analyze non-stationary nonlinear data. It is an adaptive time frequency analysis tool based on the local feature of the data in time domain. And Bidimensional Empirical Mode Decomposition (BEMD) is a better generalization of one-dimensional EMD decomposition idea in two-dimensional planes, which mainly includes the modes of one-way two-dimensional empirical decomposition [9], [10] and two-dimensional empirical mode decomposition based on radial basis function extraction envelope [11] [12] [61]. Although these algorithms have been successfully applied in some aspects, they have a common defect. The decomposed intrinsic mode function components contain too bright and too dark areas, so-called "grayscale spots", which is because of the strong nonlinear time-varying characteristics of the image and the overshoot and undershoot of the interpolation functions used. These grayscale spots have a very adverse effect on the subsequent processing of the image. The above various decomposition algorithms do not impose certain restrictions on the decomposition, resulting in the uncertainty of the frequency in the same decomposition (there is no limit bandwidth in the same decomposition). That is meaning that as long as the EMD decomposition condition can be decomposed, regardless of the difference of frequency, the pattern is mixed, so the result will appear "gray spot" in the same decomposition. In order to better understand the related work of near-infrared image enhancement for readers, we summarize them in mind map, as shown in Fig. 2.

How to better understand and master the optical properties of near-infrared biological tissue, more perfect near-infrared imaging technology and image processing algorithms is still

an open field of study [49] [58] [59]. The economical, reliable, clear imaging near-infrared detection equipment [60] and the excellent near-infrared image processing software not only can deeply understand the near-infrared imaging detection technology, but also has a broad market application prospects.

III. Near-infrared Image Enhancement Method Based on Steerable Pyramid

In this section, we introduce and analyze the near-infrared image enhancement method in IRFPA based on the steerable pyramid in detail, and then demonstrate the rationality of the algorithm from many aspects. Each section introduces a flow of the algorithm

A. Steerable Pyramid

The steerable pyramid algorithm is a reversible multi-scale image transformation algorithm [7], [8]. The transformation process of the manipulated pyramid decomposition theory is similar to the tower structure that used in orthogonal wavelet multi-resolution analysis, and the image is decomposed into the sub-band information with different scales and different directions. Through the decomposed sub-band images, we can observe and analyze the features we need from different scales and in different directions. The difference is that the manipulated pyramid decomposition uses the same number of directional filters in all pyramid layers, which greatly reduces the amount of data that is calculated and stored.

According to the sampling theorem [23], it is necessary to eliminate all fine structures obtained by one-fourth sampling of less than the shortest wavelength by smoothing filters, so that a correct sub-sampling image can be obtained. From the scale space point of view, this indicates that the reduction of the size of images needs to be synchronized with the proper smoothing of the image. If the smooth and sub-sampling are repeated, a series of image pyramids can be formed (*e.g.*, Gaussian Pyramid). In the pyramid image series, the image of each layer is half the width and height of the next layer, and the size of the image decreases with the increase of the number of layers. The missing information between the two-stage Gaussian pyramid needs to be obtained by interpolation. Therefore, it is necessary to introduce the insertion filter to determine the approximate degree between the predicted value and the input image. If the insertion filter is ignored, the predicted value will be the interpolation form of the input image, and the block effect of the duplicated pixel will become apparent. The insertion filter needs to double the size of the image in all directions, with one value inserted between any two pixels in each row and one line between each row. Laplace pyramid [50], [51] is the difference image between Gaussian pyramid and its upper layer by interpolation, which reflects the information difference between the two levels of Gaussian pyramid. In fact, it is the detail part of the image.

The purpose of the pyramid decomposition is to separate the source images into different spatial frequency bands. Then the fusion process is performed separately on every spatial frequency layer, so that the features and details on different frequency bands of different decomposition layers can be targeted. The use of different fusion operators can achieve the purpose of highlighting features and details in a particular frequency band, *i.e.*, it is possible to fuse features and details from different images.

The block diagram of one layer in the manipulated pyramid decomposition and reconstruction are shown in Fig. 3. In the graph, $H1\_1(u,v)$ represents the high-pass filter, $L1\_1(u,v)$ represents the low-pass filter, u and v are frequency-domain variables. $B1\_1(u,v)\cdots B1\_k(u,v)$ are directional band-pass filters, which outputs k directional filtering results. $L1\_2(u,v)$ is a low-pass filter corresponding to the band-pass filter and outputs the low frequency information of the current scale. The variables outside the frame represent the input and output images. The up and down arrows represent the up and down sampling of the image with a stride of 2×2. Ellipsis partially repeats the block diagram, which is the critical point between adjacent scales, and is also the division of the current scale decomposition and reconstruction. In order to ensure that the image information is not lost, the above filter banks must satisfy the following three conditions:

- Flat system response, *i.e.*,

$$|H1\_1(u,v)|^2+|L1\_1(u,v)|^2\left(|L1\_2(u,v)|^2+|B1\_1(u,v)|^2+\cdots+|B1\_k(u,v)|^2\right)=1 \tag{1}$$

- Recursion cycle, *i.e.*,

$$|L1\_2(\frac{u}{2},\frac{v}{2})|^2=|L1\_2(\frac{u}{2},\frac{v}{2})|^2\left(|L1\_2(u,v)|^2+|B1\_1(u,v)|^2+\cdots+|B1\_k(u,v)|^2\right) \tag{2}$$

- No aliasing, *i.e.*,

$$L1\_2(u,v)=0,\ s>f_N/2 \tag{3}$$

where f_N is Nyquist sampling frequency and $s=\sqrt{u^2+v^2}$ is frequency domain radius.

During the experiments, we use the following filter banks:

(1) Low-pass filter is defined as

$$LP(a,b,f)=\begin{cases}1 & , \quad f\le a\\ \sqrt{\frac{1}{2}\left[1+\cos[\pi(\frac{f-a}{b-a})]\right]} & , \quad a<f<b\\ 0 & , \quad f\ge b\end{cases} \tag{4}$$

$$L1\_1(u,v)=LP(f_2,f_N,s) \tag{5}$$

$$L1\_2(u,v)=LP(f_1,f_N/2,s) \tag{6}$$

where a and b determine the band limit of the low pass filters. f_1, f_2, and f_N are manually defined hyper-parameters in the process of experiments.

(2) High-pass filter is defined as

$$HP(a,b,f)=\begin{cases}0 & , \quad f\le a\\ \sqrt{\frac{1}{2}\left[1+\cos[\pi(\frac{f-a}{b-a})]\right]} & , \quad a<f<b\\ 1 & , \quad f\ge b\end{cases} \tag{7}$$

$$H1\_1(u,v) = HP(f_2, f_N, s) \tag{8}$$

$$H1\_2(u,v) = HP(f_1, f_N / 2, s) \tag{9}$$

(3) Directional band-pass filter:

The formula of k directional filter is defined as

$$B1\_m(u,v) = H1\_2(u,v) * \cos^{k-1}(\theta - nm\pi / k) \tag{10}$$

where

$$\theta = \tan^{-1}(v / u) \tag{11}$$

where m = 0, 1, … , k-1.

B. Low-Pass Coefficient Processing

Low pass coefficients retain the general features of the original image. In this paper, we use fuzzy set theory [9] to deal with the low pass coefficients of all scales to enhance image contrast. The main steps of its theory are as follows:

(1) First, we transform image into fuzzy domain by linear membership function. The linear membership function is selected as

$$\mu_{ij} = \frac{x_{ij} - x_{\min}}{x_{\max} - x_{\min}} \tag{12}$$

where x_{max} and x_{min} represent the maximum and minimum values of the original image pixels, respectively. x_{ij} is the pixel value of each point. The membership function normalize the pixel value of digital image to 0 and 1.

(2) Then, the fuzzy contrast is calculated according to the following equation:

$$F_c = \left| \frac{\mu_{ij} - \overline{\mu}_{ij}}{\mu_{ij} + \overline{\mu}_{ij}} \right| \tag{13}$$

(3) The transformation function $\psi(x)$ are selected to stretch the grayscale of the image to complete the nonlinear transformation of fuzzy contrast [10], which satisfies the following equation:

$$\begin{cases} \psi(0) = 0 \\ \psi(1) = 1 \\ \psi(x) \geq x, x \in (0,1) \end{cases} \tag{14}$$

where $\psi(x)$ is defined as

$$\psi(x) = 4x - 6x^2 + 4x^3 - x^4 \tag{15}$$

$$F_c' = \psi(F_c) \tag{16}$$

(4) Inverse transformation: the value of the fuzzy contrast is processed and transformed by the transformation function

X11	X12	X13	X14	X15	X16		0	0	0	0	0	0
X21	X22	X23	X24	X25	X26	down-sampling	0	X22′	0	X24′	0	X26′
X31	X32	X33	X34	X35	X36		0	0	0	0	0	0
X41	X42	X43	X44	X45	X46		0	X42′	0	X44′	0	X46′
X51	X52	X53	X54	X55	X56	interpolation	0	0	0	0	0	0
X61	X62	X63	X64	X65	X66		0	X62′	0	X64′	0	X66′

Fig. 4. Schematic diagram of adaptive interpolation.

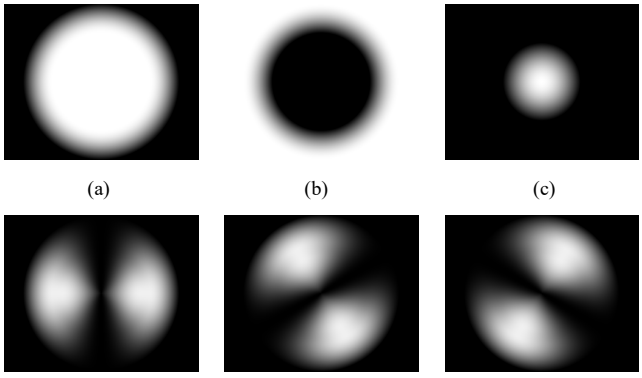

Fig. 5. Filter bank schematic diagram of the first scale. (a) L1_1; (b) H1_1; (c) L1_2; (d) B1_1; (e) B1_2; (f) B1_3.

in the step (3). Then we get the image pixel value after the transformation of fuzzy contrast by inverse transformation, according to

$$\mu_{ij}' = \begin{cases} \dfrac{\overline{\mu}_{ij}(1 - F_c')}{1 + F_c'} & , \quad \mu_{ij} \leq \overline{\mu}_{ij} \\ 1 - \dfrac{(1 - \overline{\mu}_{ij})(1 - F_c')}{1 + F_c'} & , \quad \mu_{ij} > \overline{\mu}_{ij} \end{cases} \tag{17}$$

$$x_{ij}' = \mu_{ij}'(x_{\max} - x_{\min}) + x_{\min} \tag{18}$$

C. High-Pass Coefficient Processing

During image processing, the high frequency coefficients preserves the detailed information of original image, which is usually accompanied by noises. Therefore, in this paper, we use the threshold method to deal with the coefficients of high frequency. In the high frequency coefficient, the image signal is generally larger and the noise signal is usually smaller. Therefore, through choosing the appropriate hard threshold, the signal coefficient and noise figure can be separated by the threshold function [62].

The results of threshold processing are mainly determined by two factors: the threshold size and threshold function. The selection of threshold is usually based on general threshold rule [11]:

$$\lambda = \sigma\sqrt{2\ln(n)} \tag{19}$$

where σ represents the mean square deviation of noise signal

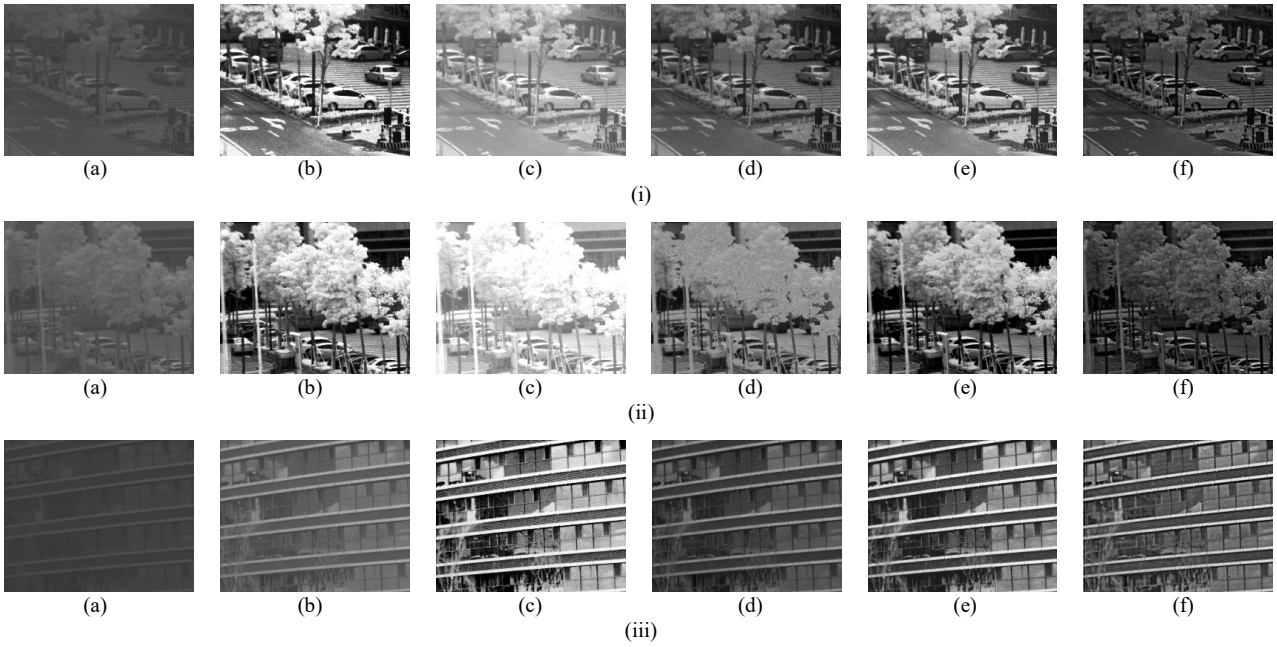

Fig. 6. Enhanced results of three scenarios in different algorithms. (a) original image; (b) histogram equalization; (c) gray stretch; (d) method in paper [5]; (e) method in paper [36]; (f) proposed algorithm.

and n is the signal length of the steerable pyramid. The mean square error of the noise signal is estimated by the median of high frequency coefficients as

$$\sigma = \text{median}(I) \tag{20}$$

The selected threshold is the minimum value of the minimum scale high frequency coefficient threshold. Then the threshold function is set to hard threshold function [12]: when the signal value is greater than the threshold, it remains unchanged, and when it is less than the threshold, it is set to zero. It is defined as

$$y = \begin{cases} x & , \ |x| \geq \lambda \\ 0 & , \ |x| < \lambda \end{cases} \tag{21}$$

Because there is a large difference in the input image itself, the fixed threshold must not have the best effect on all images. Experiments show that this fixed threshold is better for most image processing. However, if the threshold is fine-tuned, the image quality can be further improved.

D. Adaptive Interpolation

In fact, the traditional interpolation algorithms such as the zero interpolation [34], bilinear interpolation [35], and cubic interpolation [13] both have their own advantages, but they usually fail to restore the high-frequency information of the image. In the steerable pyramid based algorithms, the above interpolation methods will lead to large distortion of the final image reconstruction results. Therefore, aiming at the above problem, we propose an adaptive interpolation method which can effectively reduce the up sampling distortion and achieve significant results.

The data of the even-numbered columns of the original image is down-sampled, and the ratio of the data of the culled data (called non-retained values) to the average value of the even-numbered columns (called retention values) in the surrounding 3×3 fields is recorded [53], [54]. After the zero-interpolation of the up-sampled interpolator, the value of each zero is reassigned. The size of the new assignment is determined by the ratio of the average value of retained outputs in the surrounding neighborhood (with a windows size of 3×3) and the ratio recorded in the down-sampling process. As shown in Fig. 4, the ratio of the data X_{33}, X_{43} in the down-sampling process to the average of the retention values in the 3×3 neighborhood is

$$r_{33} = \frac{X_{33}}{(X_{22} + X_{24} + X_{42} + X_{44})/4} \tag{22}$$

$$r_{43} = \frac{X_{43}}{(X_{42} + X_{44})/2} \tag{23}$$

Then the updated new sample of this position $X33'$ and $X43'$ are

$$X'_{33} = r_{33} * (X'_{22} + X'_{24} + X'_{42} + X'_{44})/4 \tag{24}$$

$$X'_{43} = r_{43} * (X'_{42} + X'_{44})/2 \tag{25}$$

E. Anti-sharpening Mask

As shown in Fig. 3, after reconstructing the image, we use the anti-sharpening mask algorithm to compensate for the unavoidable details loss. The anti-sharpening mask algorithm is defined as

$$v = x + \gamma(x - y) \tag{26}$$

where v represents an enhanced image and x represents an input image I_r. y is the result of the linear low pass filter,

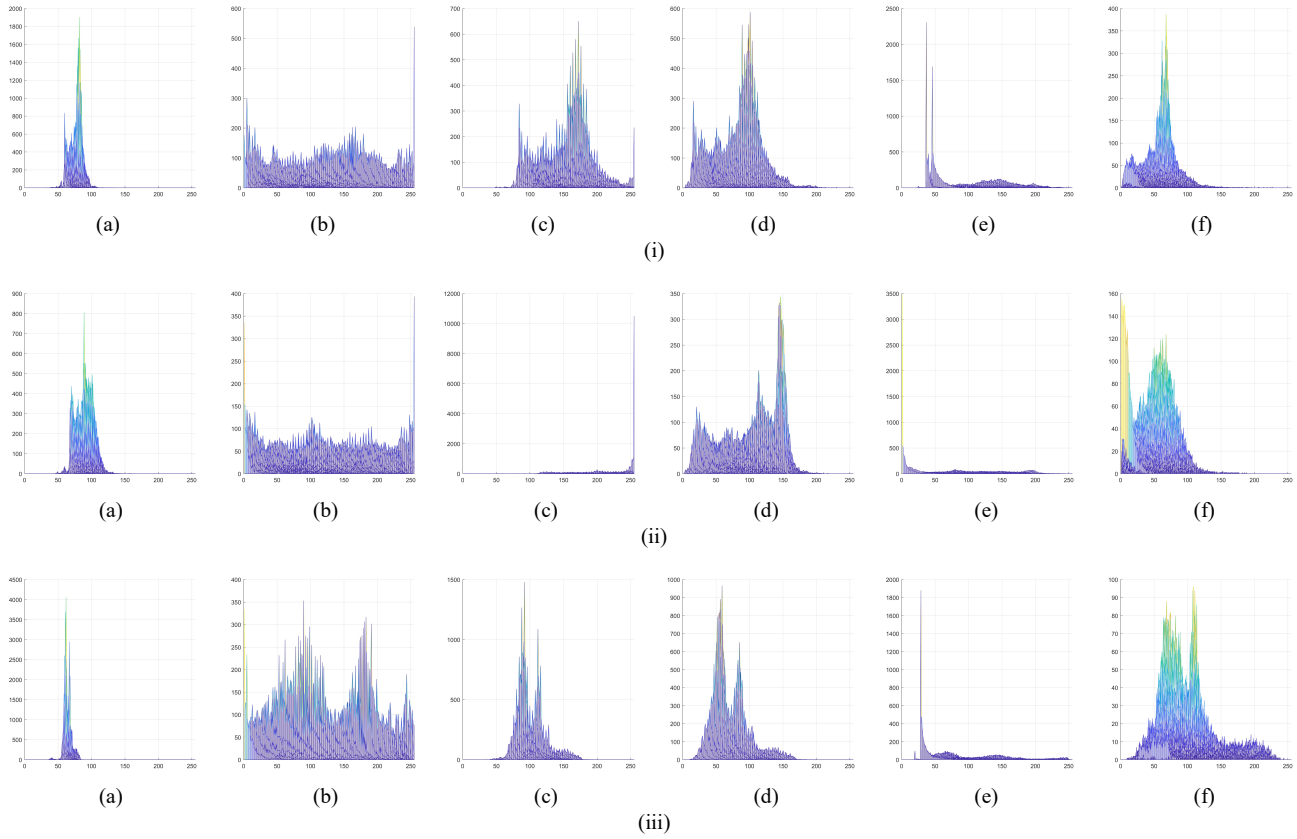

Fig. 7. The grayscale histogram of each enhanced result of three scenarios in different algorithms. (a) original image; (b) histogram equalization; (c) gray stretch; (d) method in paper [5]; (e) method in paper [36]; (f) proposed algorithm.

which uses the filter L_{1_2} in the first layer of steerable pyramid. γ (γ>0) is the weighting factor, which is selected as 1 in this paper.

IV. Experimental Results and Analysis

In this part, we describe the algorithm flow and parameter settings in the experimental process, and finally compare the subjective effects and objective evaluation criteria of each algorithm on datasets.

In this paper, 3 layers of pyramid decomposition method is adopted. Each layer selects k (k=3) directions, which are 60°, 80°, and 120°, respectively. The size of the input image is 256×320. The visualization results of each filter (take the first level as an example) are shown in Fig. 5.

A. Subjective Evaluation

Subjective evaluation generally considers image quality to the extent that an image under test (*i.e.*, a target image) produces an error in the human visual system relative to a standard image (*i.e.*, the original image). In other words, compared with the original image, the human eye thinks that the target image has almost no degradation or damage, and the quality of the target image is high, otherwise the image quality is poor [52]. Another definition is that in the absence of the original image, the human eye can clearly distinguish the things in the image, and the foreground and the background in the image, the outline of the object, the texture, etc., which can be better differentiated, then the image quality is good. Otherwise, the image quality is poor.

In this part, we show the image enhancement results of the three sets of scenes. Each experiment is compared with the proposed algorithm in five methods, which are histogram equalization, gray stretch, and infrared image enhancement with histogram equalization and fuzzy set theory to enhance [5]. The experimental results of various methods are shown in Fig. 6.

In Fig. 6 (i)-(a), it shows the original near-infrared image of the first scene that formed by the device NIR-50. This image has undergone the removal of blind pixels and non-uniformity correction. It can be seen from the figure that the original image has low contrast, blurred image and poor visual effect. Fig. 6 (i)-(b) shows the results of the histogram equalization. The over-enhancement of the image leads to a large loss of detail information in the original image. Fig. 6 (i)-(c) shows the results of the grayscale stretching process of the image, and the grayscale stretching has the significant enhancement effect compared to the original image. The image resolution is good, but the image still has a lot of noise, and some details are not obvious. Fig. 6 (i)-(d) shows the results of the infrared image enhancement algorithm in the [5], [55] combined with histogram equalization and fuzzy set theory. It can be seen that the image is bright but the noise is obvious. Fig. 6 (i)-(e) shows the enhancement results of the hybrid method [36] combining the color information, information of entropy, and 16-neighborhood local features. It overemphasizes details and causes distortion in image contrast. Fig. 6 (i)-(f) is the result of the algorithm that proposed in this paper. It can be

TABLE I
FOUR KINDS OF OBJECTIVE INDICATOR DATA OF SCENE I THAT PROCESSED BY DIFFERENT ALGORITHMS

Methods	Contrast gain	Comentropy	MSE	PSNR
Original	1.00	5.19	---	---
Histogram	6.33	5.04	6839.5	9.79
Gray stretch	3.88	5.19	782.5	19.19
Yun *et al.* [5]	3.88	5.94	4146.0	11.95
Guo *et al.* [36]	3.27	6.02	1223.5	8.24
Lin *et al.* [41]	5.10	6.74	1384.3	10.84
Yeom [42]	2.41	3.99	5524.1	5.49
Li *et al.* [43]	1.98	4.51	943.3	7.22
Dubey [44]	3.96	5.50	3152.2	13.61
Xu *et al.* [45]	2.50	5.64	2004.2	10.40
Cao *et al.* [46]	3.36	4.22	952.4	7.85
Qi *et al.* [47]	5.11	4.32	3371.2	9.28
Zhu *et al.* [48]	2.04	3.19	1052.2	8.57
Our method	**6.59**	**6.84**	**708.8**	**19.63**

TABLE II
FOUR KINDS OF OBJECTIVE INDICATOR DATA OF SCENE II THAT PROCESSED BY DIFFERENT ALGORITHMS

Methods	Contrast gain	Comentropy	MSE	PSNR
Original	1.00	5.70	---	---
Histogram	5.27	5.53	5124.9	11.03
Gray stretch	3.37	5.49	1479.1	16.43
Yun *et al.* [5]	3.88	**6.90**	1870.0	15.41
Guo *et al.* [36]	6.56	6.11	2239.2	11.20
Lin *et al.* [41]	6.24	6.48	2642.1	12.35
Yeom [42]	2.95	3.39	1992.4	8.84
Li *et al.* [43]	2.02	5.02	1924.1	9.22
Dubey [44]	4.83	6.08	1552.9	13.59
Xu *et al.* [45]	2.57	5.66	1362.7	14.27
Cao *et al.* [46]	4.15	3.83	1594.3	7.79
Qi *et al.* [47]	2.33	5.34	1221.0	10.19
Zhu *et al.* [48]	3.88	4.40	3258.1	11.67
Our method	**6.91**	6.84	**1124.0**	**16.03**

TABLE III
FOUR KINDS OF OBJECTIVE INDICATOR DATA OF SCENE III THAT PROCESSED BY DIFFERENT ALGORITHMS

Methods	Contrast gain	Comentropy	MSE	PSNR
Original	1.00	4.45	---	---
Histogram	6.71	4.32	8769.2	8.70
Gray stretch	4.61	4.44	3794.7	19.12
Yun *et al.* [5]	6.65	6.45	5051.8	11.10
Guo *et al.* [36]	3.27	5.13	3951.1	8.95
Lin *et al.* [41]	4.47	5.52	2741.5	5.95
Yeom [42]	3.28	7.03	3225.4	18.22
Li *et al.* [43]	3.91	6.44	2053.0	14.27
Dubey [44]	5.94	5.45	3337.5	12.67
Xu *et al.* [45]	3.23	4.22	2532.1	8.05
Cao *et al.* [46]	4.19	7.22	4585.2	13.24
Qi *et al.* [47]	3.65	5.57	3696.7	11.94
Zhu *et al.* [48]	3.81	3.98	3521.4	7.22
Our method	**7.12**	**7.46**	**1997.9**	**19.36**

TABLE IV
COMPARISON OF SINGLE IMAGE PROCESSING SPEED OF VARIOUS ALGORITHMS

Algorithms	Platform	Time/frame (s)
Original	---	---
Histogram	Matlab	**0.4**
Gray stretch	Matlab	1.5
Yun *et al.* [5]	Matlab	4.2
Guo *et al.* [36]	C/C++	2.7
Lin *et al.* [41]	Matlab	3.9
Yeom [42]	C/C++	**1.4**
Li *et al.* [43]	C/C++	1.9
Dubey [44]	Python	2.2
Xu *et al.* [45]	C/C++	1.1
Cao *et al.* [46]	C/C++	0.9
Qi *et al.* [47]	Python	2.0
Zhu *et al.* [48]	Matlab	3.4
Our method	Matlab	2.3

seen that the contrast of the image is improved obviously, the noise is less, and the details are more real.

Fig. 6 (ii)-(a) is the original near-infrared image of the second scene that formed by the device NIR-50, which has low contrast and blurred edges. Fig. 6 (ii)-(b) shows the result of the histogram equalization. The gray scale is larger and the image is too bright, resulting in the loss of detail. Fig. 6 (ii)-(c) is the grayscale stretch result, from which we can see that a lot of detail information is obviously lost. The result of Fig. 6 (ii)-(d) shows that the brightness is greatly improved, but the brightness is not balanced, such as the difference between the brightness of the leaves and the trunk. Method in [36] results in the abnormal illumination (Fig. 6 (ii)-(e)). The algorithm proposed in this paper (in Fig. 6 (ii)-(f)) highlights the detail information while preserving the original brightness ratio of the image, and has obvious improvement effect.

Fig. 6 (iii)-(a) shows the original near-infrared image of the third scene that formed by the device NIR-50. It can be seen that the image is dark, the details are blurred, and the visual effect is poor. Fig. 6 (iii)-(b) shows the histogram equalization results. The overall scene is bright, and the trees in the lower right are too bright and distorted. Fig. 6 (iii)-(c) shows the result of grayscale stretch method, which has a low contrast and blurred details. There is a bad phenomenon of uneven brightness in the result of Fig. 6 (iii)-(d). Similarly, method in [36] (Fig. 6 (iii)-(e)) enhances the details of the image and also brings noise. Fig. 6 (iii)-(f) shows the result of our proposed algorithm. It can be seen that the gray changes are more uniform, the contrast changes most obviously, and the images have the best visibility.

B. Grayscale Histogram

The grayscale histogram is a function reflecting gray level distribution and is a statistic of the gray level distribution in the image. The purpose of gray histogram is to count all the pixels in the digital image according to the size of the gray value. And a grayscale histogram is the function of grayscale value, which represents the number of pixels in a picture that have a certain gray level, reflecting the frequency at which a certain gray level appears in the image.

In this section, in order to observe the changes brought by different enhancement algorithms to the original image, we counted the grayscale histogram of each result to observe the connections and differences between different algorithms, as shown in Fig. 7. Each grayscale histogram corresponds to the image of the corresponding experimental result in Fig. 6. Graphs (i), (ii), and (iii) correspond to the three scenarios, respectively.

Observing the graphs (i)-(b), (ii)-(b) and (iii)-(b) of three scenarios, it can be seen that the histogram equalization loses a large amount of image information, and the enhancement results of the natural image is completed without difference. Grayscale stretching also ensures that the original distribution does not change, but in some cases it fails (*e.g.*, Fig. 7 (ii)-(c)). The distribution of the method in [36] results in an extreme

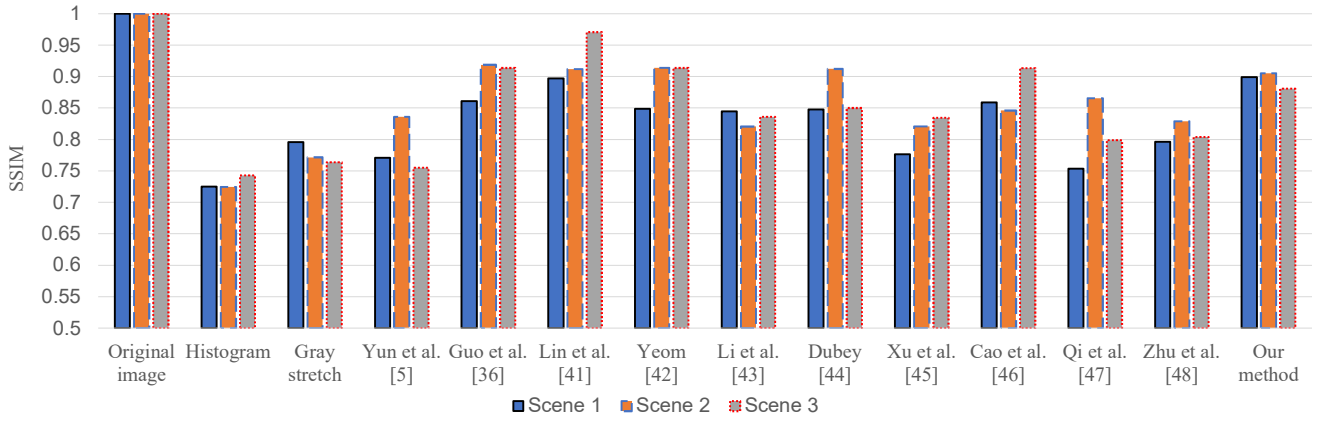

Fig. 8. The SSIM performance of various image enhancement algorithms in three scenarios. The first, the second, and the third column represent the SSIM values of Scene 1, Scene 2, and Scene 3, respectively.

unimodal phenomenon (*i.e.*, in Fig. 7 (i)-(d), Fig. 7 (ii)-(d), and Fig. 7 (iii)-(d)) that over-emphasizes some of the details and causes partial distortion of the image. Compared to each natural image in the same scenario, it can be clearly seen that the maximum degree of the obtained gray histogram of the enhancement results obtained by our algorithm preserves the distribution of the original image and makes a certain degree of change. We think that these changes are the key to achieve image enhancement. Therefore, we should strengthen the detailed information of the image based on preserving the general information, so as to achieve the purpose of natural image enhancement.

C. Objective Evaluation

Objective evaluation method refers to comparing the local differences between the distorted image and the reference image by designing features, then finding a total average statistic over the entire image, and correlating this statistic with the image quality.

The most commonly used quality evaluation algorithms are Mean Squared Error (MSE) [37] and peak signal-to-noise ratio (PSNR) [38]. MSE is defined as

$$MSE = \frac{1}{n}\sum_{i=1}^{n} w_i (f_i - \hat{f}_i)^2 \tag{27}$$

where f and $\hat{f}$ represent the original image and the enhanced image, respectively. Then the PSNR is defined as

$$PSNR = 10\log_{10}\left[\frac{\sum_{x=1}^{N_x}\sum_{y=1}^{N_y} 255^2}{\sum_{x=1}^{N_x}\sum_{y=1}^{N_y}(f(x,y)-\hat{f}(x,y))^2}\right] = 10\log_{10}\left[\frac{255^2}{MSE}\right] \tag{28}$$

MSE and PSNR are two widely used index in the image processing because of their small computational complexity and easy implementation. But the drawback is that there is no necessary connections between the output value given and the perceived quality of the sample image. Comenentropy [39] is a measure of the amount of information needed to eliminate uncertainty, *i.e.*, the amount of information that an unknown event may contain. It is defined as

$$H(X) = -\sum_{x\in X} P(x)\log(P(x)) \tag{29}$$

where $P(x)$ represent the probability of event $X = x$. It can be seen from the formula that information entropy is actually a mathematical expectation of information quantity of a random variable. On the other hand, the impact of contrast [40] on visual effects is very critical [56]. In general, the greater the contrast, the clearer and brighter the image, the brighter the color, and the less contrast, the whole picture will be gray. Therefore, observing and contrasting the contrast gain of each algorithm [57] has practical significance for measuring the effectiveness of the image enhancement algorithm.

The results of the objective evaluation criteria for each algorithm in the three scenarios are shown in Tables I, II, and III, respectively. All optimal values are highlighted in bold. It can be seen from Table I that the contrast of the algorithm is obviously improved and the information entropy is increased. Compared with the traditional image enhancement method and the methods MSE and PSNR in the [5], the algorithm has obvious good effects in the near-infrared image enhancement processing. In Table II, we can see that the algorithm in this paper is basically the best in all data, only the contrast gain of paper [5] is slightly greater than this algorithm, but the other three indexes are superior to the index value of paper [5], so the results of this algorithm are better. As can be seen from the data in Table III, the PSNR of the gray-scale stretched image is large, and the reason for analyzing the samples is that the gray-scale stretch does not significantly change the original image data, resulting in the smaller mean square error and the larger PSNR. The outstanding results cannot reflect absolute superiority of the method. Considering the contrast gain and information entropy, the proposed algorithm in this paper is more ideal.

The contrast gain, Comentropy, MSE, and PSNR of our proposed near-infrared image enhancement algorithm in three scenarios outperform the state-of-the-art performance with 4.2%, 5.5%, and 4.6%, 4.7%, 5.0%, and 3.9%, 4.2%, 5.3%, and 5.6%, respectively, which show the better performance of our algorithm.

Algorithm complexity refers to the resources needed for the

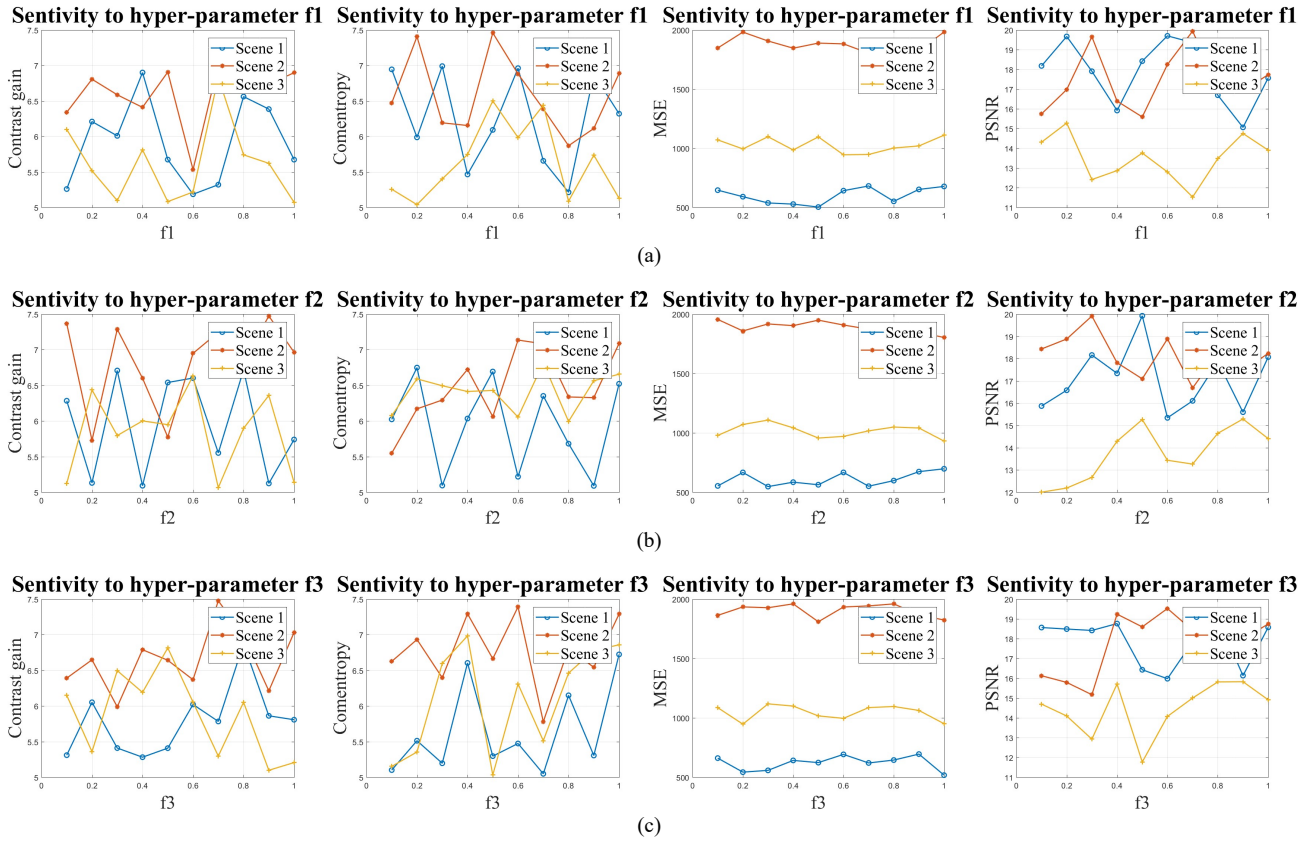

Fig. 9. The sensitivity performance (Contrast gain, Comentropy, MSE, and PSNR) of proposed algorithm in three scenarios. The first row (a), the second row (b), and the third row (c) represent the hyper-parameters f_1, f_2, and f_3, respectively.

algorithm to run when it is written into executable programs. Resources include time resources and memory resources. The time complexity of the algorithm qualitatively describes the running time of the algorithm, which is very important for the practical application of the algorithm. Therefore, we compare the processing time of different algorithms for a single image, as shown in Table IV. The algorithm implementation platform includes Matlab, Python, and C/C++, which runs under the windows 10 system. And the computer used foe extensive experiments is configured as an i7-8750H CPU, 16G RAM, 1T hard drive space, and a NVIDIA GTX 1050Ti graphics card. As we can see from the experimental results, although our algorithm has not achieved the fastest speed, the speed of 43 fps fully meets the real-time applications in most scenes.

D. Structural Similarity Index

The structural similarity index (SSIM) defines the structure information as independent of brightness and contrast, which reflects the properties of object structure in the scene, and models distortion as a combination of three different factors: brightness, contrast and structure. The mean value of SSIM is used as the luminance estimation, the standard deviation as the contrast estimation, and the covariance as the measure of the degree of structural similarity.

The SSIM of the two images **P** and **Q** can be calculated as follows:

$$\mathrm{SSIM}=\frac{(2\mu_{\mathbf{p}}\mu_{\mathbf{q}}+c_1)(2\sigma_{\mathbf{pq}}+c_2)}{(\mu_{\mathbf{p}}^2+\mu_{\mathbf{q}}^2+c_1)(\mu_{\mathbf{p}}^2+\mu_{\mathbf{q}}^2+c_2)} \tag{30}$$

where

$$c_1=(k_1L)^2$$
$$c_2=(k_2L)^2$$

where μ represents the mean value, σ represents the variance, and $\sigma_{\mathbf{pq}}$ represents the covariance. c_1 and c_2 are constants used to maintain stability, in which k_1=0.01 and k_2=0.03. L is the dynamic range of pixel values. The structural similarity index ranges from -1 to 1, and the value of SSIM equals 1 when two images are identical.

Then, we compare the SSIM performance of various image enhancement algorithms in three scenarios, as shown in Fig. 8. It can be clearly seen that our proposed algorithm achieves the acceptable SSIM value in the three scenarios (*i.e.*, 0.89, 0.91, and 0.88), which illustrates the superiority of our proposed algorithm (our proposed algorithm can improve the quality of the image based on slightly changing the image.).

E. Hyper-parameters Sensitivity

In the processing of near-infrared image enhancement, the algorithm introduces three hyper-parameters f_1, f_2, and f_N with a range of (0, 1). The selection of hyper-parameters is of great significance to the enhancement capability of our proposed algorithm, which determines the practical application value of the algorithm. Therefore, in this section, we observe the robustness of the algorithm to the hyper-parameters according to the objective evaluation criteria. The sensitivity of the algorithm to hyper-parameters in the three scenarios is shown in Fig. 9 where (a), (b), and (c) represent the evaluation results of three hyper-parameters f_1, f_2, and f_N.

It can be clearly seen from the experimental results that the

algorithm is robust to the three hyper-parameters: even if the change of the hyper-parameter exceeds 0.5, the contrast gain does not change by more than 2, the change of Comentropy does not exceed 2, the change of MSE does not exceed 100, and the PSNR changes no more than 5 in three scenarios. Moreover, comparing (a), (b), and (c), the algorithm is more sensitive to f_N than f_1 and f_2, which is due to the its location in the algorithm.

V. Conclusion

Near-infrared imaging is a mainly used method in various imaging techniques, which has better atmospheric penetration performance and human skin penetration performance than other visible light imaging methods. Therefore, near-infrared imaging method is widely used in the military, medical and industrial production. This paper proves that the steerable pyramid based near-infrared image enhancement algorithm is superior to the traditional image enhancement methods in improving the performance of the image quality by theory analysis and experiments. Generally speaking, near-infrared image enhancement mainly starts from two aspects, one is to improve contrast, and the other is to reduce noise. Traditional methods often fail to take account of both two aspects. In this paper, the algorithm is proposed to improve the contrast of the low pass image by nonlinear transformation in fuzzy set in the multi-scale processing, and the high pass images utilize the threshold method to reduce the noise. To a certain extent, the above two aspects are taken into consideration in the method. The final image is used to compensate for the slight details lost in the process of anti-sharpening masking. At the same time, the adaptive up-sampling and interpolation algorithm proposed in this paper has the "memory", which is better to restore the information. It is useful to reduce the distortion in the steerable pyramid algorithm, and it is very important to the application of the whole algorithm. And experimental results illustrate that the near-infrared image enhancement method proposed in this paper is effective.

In general, extensive experimental results show that this algorithm has a good influence on the near-infrared image enhancement, and significantly improves the quality of near infrared imaging of IRFPA devices. The comparison results with various methods show that our algorithm outperforms the state-of-the-art in terms of the contrast gain, comentropy, mean-square error, and peak signal to noise ratio. The results of the experiments illustrate that the proposed algorithm efficiently enhance the image.

At the same time, the experiments and analysis point out a few lessons and future directions, which we summarize as the followings:

- In addition to subjective evaluation method, we need an objective and effective image evaluation method to evaluate the quality of enhanced images obtained by not using the method.
- In order to complete real-time computation of the image enhancement algorithm on mobile terminal devices, the time complexity needs to be further reduced.
- How to enhance the image while avoiding noise is still a key issue.

We are actively pursuing the above directions in the future studies.

References

[1] WQ. Jin, B. Liu, YJ. Fan *et al.*, "Review on Infrared Image Detail Enhancement Techniques," Infrared and Laser Engineering, vol. 40, no. 12, pp. 2521-2527, 2011.

[2] T. Celik, "Two-dimensional Histogram Equalization and Contrast Enhancement," Pattern Recognition, vol. 45, no. 10, pp. 3810-3824, 2012.

[3] Q. Zhang *et al.*, "Segmentation of hand gesture based on dark channel prior in projector-camera system," in *IEEE/CIC ICCC*, Qingdao, China, pp. 1-6, 2017.

[4] Y. Li, YF. Zhang, N. Li and *et al.*, "Adaptive Detail Enhancement for Infrared Image Based on Subband Decomposed Multi-scale Retinex," Chinese Journal of Lasers, vol. 42, no. 5, pp. 253-261, 2015.

[5] HJ. Yun, ZY. Wu, GJ. Wang *et al.*, "Enhancement of Infrared Image Combined with Histogram Equalization and Fuzzy Set Theory," Journal of Computer-Aided Design & Computer Graphics, vol. 27, no. 8, pp. 1498-1505, 2015.

[6] HG. Jia, ZP. Wu, MC. Zhu *et al.*, "Infrared Image Enhancement Based on Generalized Linear Operation and Bilateral Filter," Optics and Precision Engineering, vol. 21, no. 12, pp.3272-3282, 2013.

[7] K. Ghosh, S. Sarkar, and K. Bhaumik, "Understanding Image Structure from A New Multi-scale Representation of Higher Order Derivative Filters," Image & Vision Computing, vol. 25, no. 8, pp. 1228-1238, 2007.

[8] ASP. Department *et al.*, "Shiftable Multi-scale Transforms," IEEE Transactions on Information Theory, vol. 32, no. 2, pp. 587-607, 2012.

[9] W. Hui and J. Zhang, "Algorithm of Edge Detection Based on Fuzzy Enhancement of Contrast Among Successive Regions," Acta Electronica Sinica, vol. 28, no. 1, pp. 45-47, 2000.

[10] J. Li, W. Sun, and L. Xia, "Novel Fuzzy Contrast Enhancement Algorithm," Journal of Southeast University, vol. 34, no. 5, pp. 675-677, 2004.

[11] HJ. Dou, QL. Wang, and X. Zhang, "A Joint Estimation Algorithm of TDOA and FDOA Based on Wavelet Threshold Denoising and Conjugate Fuzzy Function," Journal of Electronics & Information Technology, vol. 38, no. 5, pp.125-135, 2016.

[12] L. Mu, H. Wang and Y. Zhang, "An Improved Wavelet Threshold Denoising Algorithm for Analyzing Signals in the XRD Spectrum," Advances in Applied Mathematics, vol. 04, no. 3, pp. 224-229, 2015.

[13] X. Fu and B. L. Guo, "Area-directed Adaptive Image Interpolation Algorithm," Journal of Optoelectronics Laser, vol. 19, no. 2, pp. 233-236, 2008.

[14] Q. Zheng *et al.*, "Fine-grained image classification based on the combination of artificial features and deep convolutional activation features," in *IEEE/CIC ICCC*, Qingdao, China, pp. 1-6, 2017.

[15] Q. Zheng, M. Yang, Q. Zhang, and J. Yang, "A Bilinear Multi-Scale Convolutional Neural Network for Fine-grained Object Classification," IAENG International Journal of Computer Science, vol. 45, no. 2, pp. 340-352, 2018.

[16] Q. Zheng, M. Yang *et al.*, "Improvement of Generalization Ability of Deep CNN via Implicit Regularization in Two-Stage Training Process," IEEE Access, vol. 6, pp. 15844-15869, 2018.

[17] Q. Zheng, M. Yang *et al.*, "Understanding and Boosting of Deep Convolutional Neural Network Based on Sample Distribution," in IEEE 2nd Information Technology, Networking, Electronic and Automation Control Conference, Chengdu, China, pp. 823-827, 2017.

[18] X. Han, A. Aysa, H. Mamt, and K. Ubul, "Script Identification of Central Asian Printed Document Images Based on Non-subsampled Contourlet Transform," Engineering Letters, vol. 25, no. 4, pp. 389-395, 2017.

[19] A. Kulyukin and S. Reka, "Toward Sustainable Electronic Beehive Monitoring: Algorithms for Omnidirectional Bee Counting from Images and Harmonic Analysis of Buzzing Signals," Engineering Letters, vol. 24, no. 3, pp. 317-327, 2016.

[20] G. Hou, G. Wang, Z. Pan, B. Huang, H. Yang, and T. Yu, "Image Enhancement and Restoration: State of the Art of Variational Retinex Models," IAENG International Journal of Computer Science, vol. 44, no. 4, pp. 445-455, 2017.

[21] H. Rassem, E. Khoo, M. Makbol, and A. Alsewari, "Multi-Scale Colour Completed Local Binary Patterns for Scene and Event Sport Image Categorisation," IAENG International Journal of Computer Science, vol. 44, no. 2, pp. 197-211, 2017.

[22] R. Maca, M. Benes, and J. Tintera, "Segmentation of MRI Images by Adaptive Degenerate Diffusion," IAENG International Journal of Applied Mathematics, vol. 45, no. 3, pp. 208-217, 2015.
[23] A. Khurram and D. W. Kammler, "Numerical Generation of Images for the Gibbs Phenomenon Near a Corner in the Plane," IAENG International Journal of Applied Mathematics, vol. 44, no. 1, pp. 15-22, 2014.
[24] W. Zhang, D. Bian, G. Zhang *et al.*, "Based on the Fourth-order Mutual Fuzzy Function of TDOA/FDOA Parameter Estimation Research," Radio Communications Technology, vol. 39, no. 1, pp. 28-31, 2013.
[25] W. Wu, C. Wang, J. Bao *et al.*, "A Wavelet Threshold De-noising Algorithm Based on Adaptive Threshold Function," Journal of Electronics & Information Technology, vol. 36, no. 6, pp. 1340-1347, 2014.
[26] A. Kim, M. Roy, F. Dadani *et al.*, "A Fiberoptic Reflectance Probe with Multiple Source-collector Separations to Increase the Dynamic Range of Derived Tissue Optical Absorption and Scattering Coefficients," Optics Express, vol. 18, no. 6, pp. 5580-5594, 2010.
[27] Q. Wang, K. Shastri, and T. J. Pfefer, "Experimental and Theoretical Evaluation of A Fiber-optic Approach for Optical Property Measurement in Layered Epithelial Tissue," Applied Optics, vol. 49, no. 28, pp. 5309-5320, 2010.
[28] L. Spinelli, F. Martelli, A. Farina *et al.*, "Calibration of Scattering and Absorption Properties of A Liquid Diffusive Medium at NIR Wavelengths. Time-resolved Method," Optics Express, vol. 15, no. 11, pp. 6589-604, 2007.
[29] D. Jo and H. Hyun, "Structure-Inherent Targeting of Near-Infrared Fluorophores for Image-Guided Surgery," Chonnam Medical Journal, vol. 53, no. 2, pp. 95-102, 2017.
[30] G. Gilboa, N. Sochen, and Y. Zeevi, "Image Enhancement and Denoising by Complex Diffusion Processes," IEEE Transactions on Pattern Analysis & Machine Intelligence, vol. 26, no. 8, pp. 1020-1036, 2004.
[31] Y. Wang, L. Zhang, and P. Li, "Local Variance-Controlled Forward-and-Backward Diffusion for Image Enhancement and Noise Reduction," IEEE Transactions on Image Processing, vol. 16, no. 7, pp. 1854-1864, 2007.
[32] J. Wanderley and M. Fisher, "Multiscale Color Invariants Based on the Human Visual System," IEEE Transactions on Image Processing, vol. 10, no. 11, pp. 1630-1638, 2001.
[33] Q. Zheng, X. Tian, M. Yang, and H. Wang, "Differential Learning: A Powerful Tool for Interactive Content-Based Image Retrieval," Engineering Letters, vol. 27, no. 1, pp. 202-215, 2019.
[34] R. Ionutiu, J. Rommes, and A. C. Antoulas, "Passivity-Preserving Model Reduction Using Dominant Spectral-Zero Interpolation," IEEE Transactions on Computer-Aided Design of Integrated Circuits and Systems, vol. 27, no. 12, pp. 2250-2263, 2008.
[35] C. Accadia, S. Mariani, M. Casaioli *et al.*, "Sensitivity of Precipitation Forecast Skill Scores to Bilinear Interpolation and a Simple Nearest-Neighbor Average Method on High-Resolution Verification Grids," Auk, vol. 133, no. 2, pp. 129-130, 2003.
[36] X. Guo, Y. Li, and H. Ling, "LIME: Low-Light Image Enhancement via Illumination Map Estimation," IEEE Transactions on Image Processing, vol. 26, no. 2, pp. 982-993, 2017.
[37] Q. Zheng *et al.*, "A multi-resolution mosaic method used for unmanned aerial vehicle (UAV) remote sensing image," Journal of Xi'an University of Posts and Telecommunications, vol. 22, no. 2, pp. 53-59, 2017.
[38] A. Hore and D. Ziou, "Image Quality Metrics: PSNR vs. SSIM," in IEEE International Conference on Pattern Recognition, Istanbul, Turkey, pp. 2366-2369, 2010.
[39] X. Zhang, C. Mei, D. Chen *et al.*, "Feature Aelection in Mixed Data: A Method Using A Novel Fuzzy Rough Set-based Information Entropy," Pattern Recognition, vol. 56, no. 1, pp. 1-15, 2016.
[40] K. Gu, G. Zhai, W. Lin *et al.*, "The Analysis of Image Contrast: From Quality Assessment to Automatic Enhancement," IEEE Transactions on Cybernetics, vol. 46, no. 1, pp. 284, 2016.
[41] H. Lin and Z. Shi, "Multi-scale Retinex Improvement for Nighttime Image Enhancement," International Journal for Light and Electron Optics, vol. 125, no. 24, pp. 7143-7148, 2014.
[42] E. Yeom, K. H. Nam, D. G. Paeng *et al.*, "Improvement of Ultrasound Speckle Image Velocimetry Using Image Enhancement Techniques," Ultrasonics, vol. 54, no. 1, pp. 205-216, 2014.
[43] B. Li and W. Xie, "Adaptive Fractional Differential Approach and Its Application to Medical Image Enhancement," Computers & Electrical Engineering, vol. 45, pp. 324-335, 2015.
[44] S. R. Dubey, S. K. Singh, and R. K. Singh, "Local Bit-Plane Decoded Pattern: A Novel Feature Descriptor for Biomedical Image Retrieval," IEEE Journal of Biomedical & Health Informatics, vol. 20, no. 4, pp. 1139-1147, 2016.
[45] P. Xu *et al.*, "Instance-Level Coupled Subspace Learning for Fine-Grained Sketch-Based Image Retrieval," in European Conference on Computer Vision, pp. 19-34, 2016.
[46] Y. Cao *et al.*, "Deep Visual-Semantic Quantization for Efficient Image Retrieval," in IEEE Conference of Computer Vision and Pattern Recognition, pp. 916-925, 2017.
[47] Y. Qi *et al.*, "Sketch-based image retrieval via Siamese convolutional neural network," in International Conference on Image Processing, pp. 2460-2464, 2016.
[48] L. Zhu *et al.*, "Unsupervised Visual Hashing with Semantic Assistant for Content-Based Image Retrieval," IEEE Transactions on Knowledge & Data Engineering, vol. 29, no. 2, pp. 472-486, 2017.
[49] S. Murala and Q. Wu, "Expert content-based image retrieval system using robust local patterns," Journal of Visual Communication & Image Representation, vol. 25, no. 6, pp. 1324-1334, 2014.
[50] S. Philipp-Foliguet, J. Gony, and P. H. Gosselin, "FReBIR: An image retrieval system based on fuzzy region matching," Computer Vision & Image Understanding, vol. 113, no. 6, pp. 693-707, 2009.
[51] J. S. Hare et al., "Semantic facets: an in-depth analysis of a semantic image retrieval system," in ACM International Conference on Image and Video Retrieval, pp. 250-257, 2007.
[52] I. J. Jacob, K. G. Srinivasagan, and K. Jayapriya, "Local Oppugnant Color Texture Pattern for Image Retrieval System," Pattern Recognition Letters, vol. 42, no. 1, pp. 72-78, 2014.
[53] K. Zagoris, K. Ergina, and N. Papamarkos, "A Document Image Retrieval System," Engineering Applications of Artificial Intelligence, vol. 23, no. 6, pp. 872-879, 2010.
[54] M. R. Azimisadjadi, J. Salazar, and S. Srinivasan, "An adaptable image retrieval system with relevance feedback using kernel machines and selective sampling," IEEE Transactions on Image Processing, vol. 18, no. 7, pp. 1645-1659.
[55] C. Liu *et al.*, "A content-based CT lung image retrieval system for assisting differential diagnosis images collection," IEEE International Conference on Multimedia and Expo, pp. 174-177, 2001.
[56] V. P. M. Rallabandi and S. Sett, "Image retrieval system using R-tree self-organizing map," Data & Knowledge Engineering, vol. 61, no. 3, pp. 524-539, 2007.
[57] P. Clough and M. Sanderson, "User experiments with the Eurovision cross-language image retrieval system," Journal of the American Society for Information Science and Technology, vol. 57, no. 5, pp. 697–708, 2006.
[58] Q. Zheng *et al.*, "Static Hand Gesture Recognition Based on Gaussian Mixture Model and Partial Differential Equation," IAENG International Journal of Computer Science, vol. 45, no. 4, pp. 569-583, 2018.
[59] Q. Zheng and M. Yang, "A Video Stabilization Method based on Inter-Frame Image Matching Score," Global Journal of Computer Science and Technology, vol. 17, no. 1, pp. 35-40, 2017.
[60] Q. Zhang *et al.*, "Segmentation of Hand Posture against Complex Backgrounds Based on Saliency and Skin Colour Detection," IAENG International Journal of Computer Science, vol. 45, no. 3, pp. 435-444, 2018.
[61] H. Zhuang, M. Yang, Z. Cui, and Q. Zheng, "A Method for Static Hand Gesture Recognition Based on Non-Negative Matrix Factorization and Compressive Sensing," IAENG International Journal of Computer Science, vol. 44, no. 1, pp. 52-59, 2017.
[62] Q. Zheng *et al.*, "An end-to-end image retrieval system Based on gravitational field deep learning," in IEEE International Conference on Computer Systems, Electronics and Control (ICCSEC), Dalian, China, pp. 936-940, 2017.

Qinghe Zheng was born in Jining, Shandong, China in 1993. He received his B.S. degree from Xi'an University of Posts and Telecommunications in 2014 and M.S. degree from Shandong University in 2018. Now, he is studying for his Ph.d in Shandong University. His research direction is computer vision and machine learning.